How to cite: Angew. Chem. Int. Ed. 2024, e202402449
doi.org/10.1002/anie.202402449

Noncovalent Interactions

Induced Chirality in Canthaxanthin Aggregates Reveals Multiple Levels of Supramolecular Organization

Monika Halat, Grzegorz Zając, Valery Andrushchenko, Petr Bouř,* Rafal Baranski, Katarzyna Pajor, and Malgorzata Baranska**

Abstract: Carotenoids tend to form supramolecular aggregates via non-covalent interactions where the chirality of individual molecules is amplified to the macroscopic level. We show that this can also be achieved for non-chiral carotenoid monomers interacting with polysaccharides. The chirality induction in canthaxanthin (CAX), caused by heparin (HP) and hyaluronic acid (HA), was monitored by chiroptical spectroscopy. Electronic circular dichroism (ECD) and Raman optical activity (ROA) spectra indicated the presence of multiple carotenoid formations, such as H- and J-type aggregates. This is consistent with molecular dynamics (MD) and density functional theory (DFT) simulations of the supramolecular structures and their spectroscopic response.

Carotenoids are potent antioxidants that protect cells against the harmful effects of free radicals.[1] They are widespread in nature, taking part in the pigmentation of plants and animals and redox processes, including photosynthesis. Whether chiral or not, carotenoids can aggregate and adopt ordered supramolecular structures that are typically "H-type" or "J-type".[2–4] A supramolecular chirality can be generated by chiral molecules, a combination of chiral and achiral components, or even by spontaneous organisation of non-chiral elements.[5–8] For chiral carotenoids, the supramolecular geometry strongly depends on the monomers, as has been reported for astaxanthin,[9,10] lutein,[11] and zeaxanthin.[12] Non-chiral carotenoids produce chiral systems in the presence of chiral seeds.[13] For example, induced supramolecular chirality is generated by a strong interaction between chiral (α-carotene, astaxanthin) and non-chiral (β-carotene) components. This has been described for natural microcrystals and several model aggregates following the "sergeant and soldier" rule.[13] Achiral carotenoids[3] and similar molecules[5,14] do not form chiral assemblies spontaneously, and their aggregates are racemic. However, their symmetry can be broken, e.g., by chiral solvents.[6,15–17] Alternatively, external stimuli sometimes trigger chirality at the supramolecular level.[14] These include hydro-dynamic flows caused by mechanical stirring,[18,19] photo-irradiation using circularly polarised light,[20,21] and magnetic fields.[22]

In this paper, we report chiral supramolecular formations of a non-chiral carotenoid, canthaxanthin (CAX), triggered by glycosaminoglycans (GAGs): heparin (HP) and hyaluronic acid (HA) (Scheme 1). To our knowledge, this type of chirality induction has not been previously observed.

CAX is a dark-red keto-carotenoid occurring in algae, fish, and birds.[23] It can accumulate in the macular membrane, forming crystals and causing retinopathy.[24]

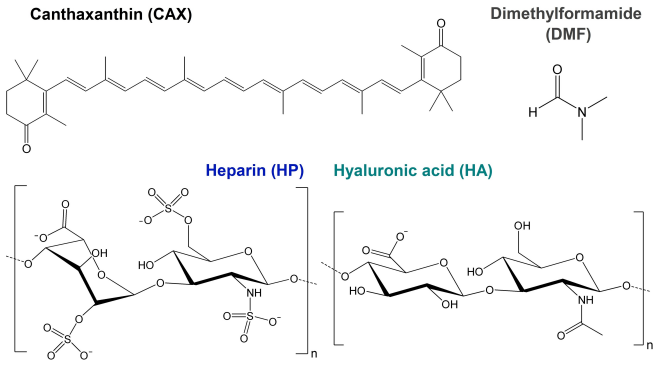

Scheme 1. Structures of the components used in the preparation of CAX-H_2O, CAX-HP and CAX-HA aggregates.

[*] Dr. M. Halat, Prof. Dr. hab. Eng. R. Baranski
Department of Plant Biology and Biotechnology
University of Agriculture in Krakow
Al. Mickiewicza 21, 31-120, Krakow, Poland
E-mail: m.halat@urk.edu.pl

Dr. G. Zając, Prof. Dr. hab. M. Baranska
Jagiellonian Centre for Experimental Therapeutics
Jagiellonian University
Bobrzynskiego 14, 30-348 Krakow, Poland

Dr. V. Andrushchenko, Prof. P. Bouř
Institute of Organic Chemistry and Biochemistry
Czech Academy of Sciences
Flemingovo náměstí 2, 16610 Prague, Czech Republic
E-mail: bour@uochb.cas.cz

MSc K. Pajor, Prof. Dr. hab. M. Baranska
Faculty of Chemistry
Jagiellonian University
Gronostajowa 2, 30-387 Krakow, Poland
E-mail: m.baranska@uj.edu.pl

MSc K. Pajor
Doctoral School of Exact and Natural Sciences
Jagiellonian University
S. Łojasiewicza 11, 30-348 Krakow, Poland

GAGs themselves are interesting molecules widely used in the cosmetic and pharmaceutical industries. They are important ingredients of connective tissue.[25] More importantly, they can induce chirality in dyes[26–28] and promote amyloid formation,[29–31] and conformational changes in peptides.[32]

Complex arrangements of carotenoids have previously been reported for astaxanthin (J_1+J_2),[10] 3′-epi-lutein (H+J),[11] epicapsorubin (H+J),[2] and carotenoylphospholipid (H+J).[33] In this study, we detected supramolecular CAX organisation by electronic circular dichroism (ECD) and Raman optical activity (ROA) spectroscopies. These are excellent chiroptical tools[34] for monitoring structure in solution. Due to the CAX chiral aggregation, its electronic transitions changed and became resonant with the incident laser radiation used in ROA, leading to an enhanced ROA signal. This effect is known as the aggregation-induced resonance ROA (AIRROA).[9–12] The intense ECD and AIRROA bands indicate the asymmetric manner of CAX packing and could be rationalised via DFT simulations. Notably, when the resonance ROA (RROA) is measured, the signal from ECD (ECD-Raman effect)[35] must be minimised[36] or subtracted.[37]

CAX molecules aggregate after adding water to a solution of pigment in an organic solvent due to hydrophobic effects and π-π stacking interactions of polyene chains.[2–4] This can be verified by UV-vis spectroscopy due to a shift of the main absorption band ($S_0 \rightarrow S_2$ transition).[38–40] Indeed, for the CAX aggregate obtained from hydrated dimethylformamide solution (DMF:H_2O 3:7), a blue shift of the main absorption band (484→453 nm) was observed (CAX-H_2O, Figure 1). This indicates an H-type aggregate, which is a tightly packed carotenoid arrangement.[2–4] The spectra reflect energy splitting and large transition electronic dipole moments in the CAX molecules (cf., the exciton coupling theory).[41,42] Upon aggregation, the absorbance diminished to approximately half compared to the monomer spectrum. Nevertheless, no supramolecular optical activity, such as Cotton effects,[43,44] arose, and no ECD signal was detected (except for noise, Figure 1). We also observed that the CAX-H_2O aggregate was not stable. After 24 h, its UV-vis spectrum almost disappeared.

Surprisingly, CAX supramolecular self-organisation proceeds differently when supported by a chiral polysaccharide environment. Indeed, the CAX-HP and CAX-HA mixtures develop a strong optical activity at the supramolecular level, measured as the exciton-split ECD bands (Cotton effects), within 24 h of preparation (Figure 2). A (−/+/−) ECD

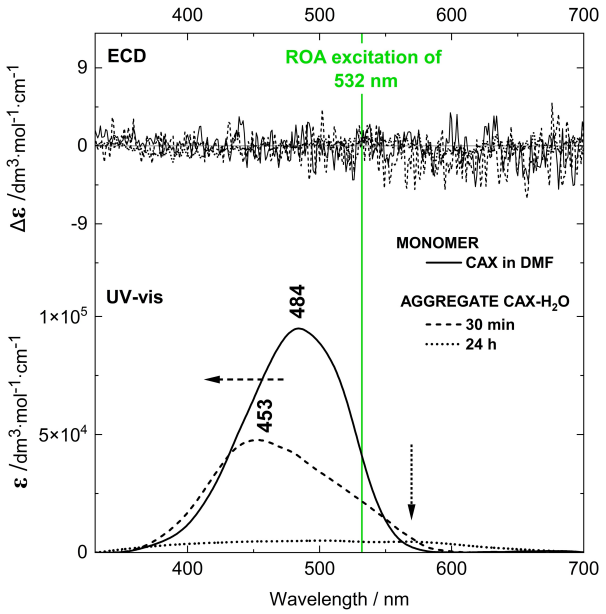

Figure 1. ECD (Δε) and UV-vis absorption (ε) spectra of the CAX-H_2O aggregate obtained after 30 min (black dashed line) and 24 h (black dotted line) of sample preparation and spectra of the CAX monomer (black solid line) in dimethylformamide (DMF).

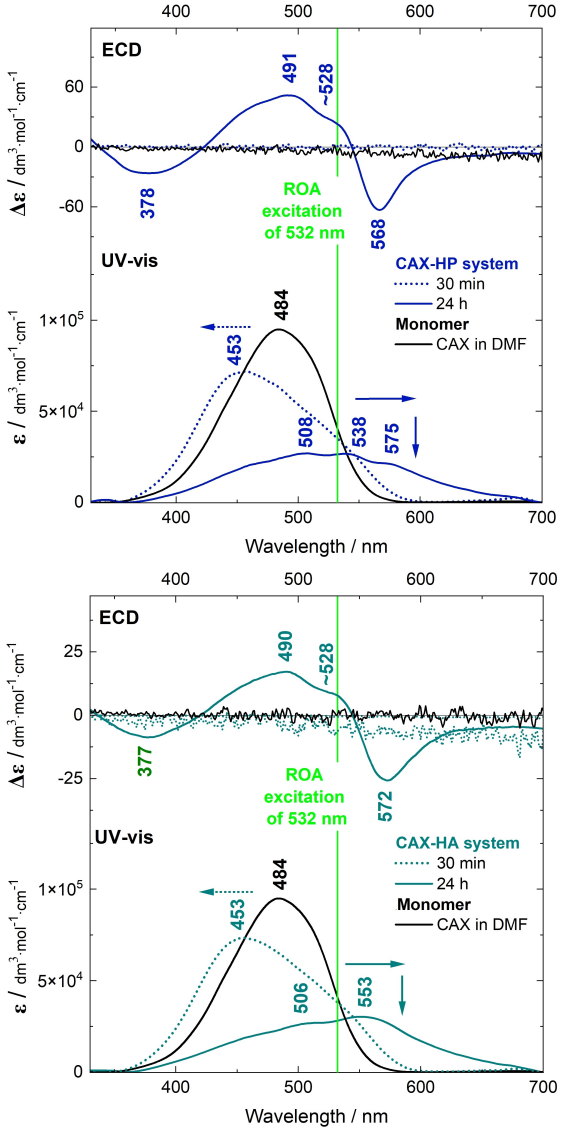

Figure 2. ECD (Δε) and UV-vis absorption (ε) spectra of the CAX-HP (blue line) and CAX-HA (cyan line) systems obtained as mixtures of CAX and GAG solutions in the ratio of 3:7 and spectra of the CAX monomer (black line) in dimethylformamide (DMF).

pattern was observed from lower to higher wavelengths, with extrema at 378/377, 491/490 and 568/572 nm for the CAX-HP/CAX-HA samples. Previous experimental[43,44] and theoretical[4,45] studies showed that the positive ECD band at ~490 nm and the negative band at ~570 nm indicate negative exciton chirality and a left-handed helical organisation. DMF:H_2O solutions of HP and HA without CAX do not exhibit measurable ECD within 330–700 nm (Figure S1 of Supporting Information, SI). Therefore, the intense ECD signals in Figure 2 can be attributed to chiral supramolecular CAX aggregates triggered and stabilised by GAGs.

However, the chirality induction is not instantaneous. The strongest optical activity appears only after 24 h. Immediately after mixing (30 min), a blue shift (484→453 nm) of the absorption maximum occurs, which later (24 h) reverses into a red shift (to 575/553 nm, Figure 2). This indicates that the CAX molecules initially aggregate through a non-chiral H-type arrangement (polyene chains are close and parallel). Subsequently, they form a more stable J-type assembly (polyene chains are further apart and in a "head-to-tail" orientation).[2–4] The red-shifted UV-vis absorption band originates from a quasi-linear mutual orientation of the transition dipole moments of the coupled polyene chains.[41,42] Thus, the structures of the CAX-HP and CAX-HA systems are complex, containing both H- and J-type substructures that become arranged in a chiral manner with time. This complexity is also reflected by the relatively rich ECD, as pure H- or J-aggregates exhibit only a bisignate couplet, and by the fine substructure of the absorption band.

Because both CAX-HP and CAX-HA aggregates strongly absorb laser light at 532 nm, the AIRROA effect is also observable (Figure 3). This makes the ROA technique (otherwise requiring much larger sample amounts) very sensitive and usable for the low-concentrated carotenoid solutions (~10^{-5} M). The RROA profiles are positive and do not follow the SES (single electronic state) limit theory suggested by Nafie.[46] According to this theory, positive ECD in the resonance wavelength generates negative ROA, proportional to the Raman spectrum. However, this cannot be applied to multiple states[47,48] or spectra involving Herzberg–Teller effects.[49] In our case, multiple states are present, as indicated by the almost continuous absorption near the 532 nm excitation line.

In principle, the ECD-Raman phenomenon[35–37] can also modulate the signs and intensities of RROA bands, i.e., experimental signal may be composed of the natural RROA and ECD-Raman parts ($I_R - I_L = RROA_{natural} + ECD\text{-}Raman$). However, in our experiments, ECD-Raman was minimised by working with low concentrations of the pigment (~10^{-5} M) and a short optical path length of light propagating through the sample.[36]

The Raman and RROA spectra of the CAX-HP and CAX-HA systems show bands typical for vibrations of the carotenoid polyene chain,[50] located at 1520/1521 (ν_1, C=C stretching), 1160/1161 (ν_2, C–C stretching), 1013 (ν_3, CH_3

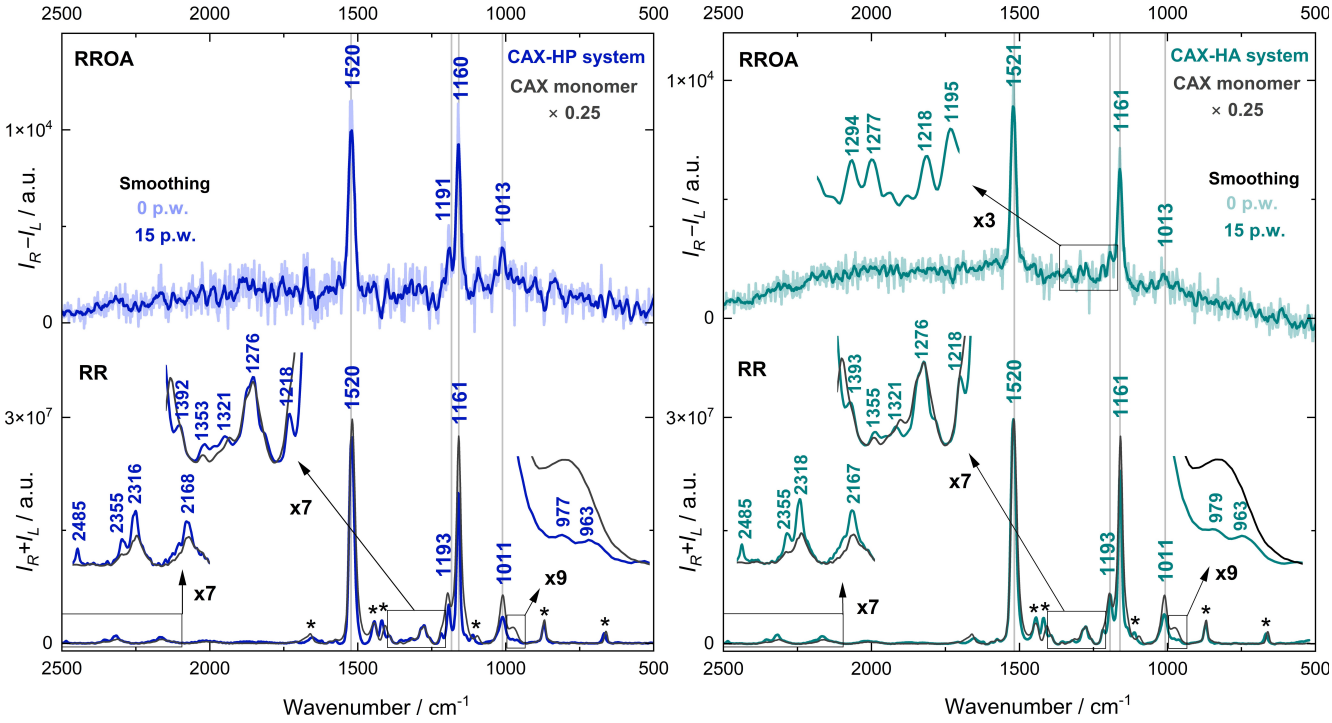

Figure 3. Experimental RROA ($I_R - I_L$) and RR ($I_R + I_L$), spectra of CAX-HP (blue line) and CAX-HA (cyan line) aggregates. RROA spectra are presented without and with the Savitzky–Golay smoothing correction with a window of 15 points (p.w.). The black line represents the RR spectrum of the CAX monomer. The intensity of the RR parts in the insets has been multiplied as indicated. RR bands originating from dimethylformamide (DMF) are marked by an asterisk (*).The intensity scales are presented in arbitrary units (a.u.).

rocking coupled with C–H bending) and 1191/1195 cm^{-1} (ν_5, C–C stretching) (Figure 3). The bands of CAX-HA observed at 1218 (ν_6, C–C and C=C stretching), 1277 (C–H rocking) and 1294 cm^{-1} (CH_3 twisting) are also attributed to the polyene chromophore vibrations. There are no visible ROA bands of HP or HA due to their low concentrations (0.05 and 0.01 mg/mL, respectively) and the weakness of non-resonance ROA. However, the RROA signals of CAX obtained for the CAX-HP and CAX-HA systems are reliable and stable and confirm the chirality induction. The normalised circular intensity difference (CID, ratio of ROA to Raman) is relatively high (~$2–3\cdot10^{-4}$) and the observed RROA is approximately proportional to the parent RR spectra. A detailed description of the positions and origins of the RROA and RR bands is presented in Table S1.

To further rationalise the chiroptical spectra and unravel the structure of the CAX-GAGs aggregates, several geometries of CAX dimers were investigated theoretically. They have different parameters affecting the absorption and ECD bands, such as inter-molecular distance (d) and torsion angle (α) (SI). Spectra of three dimer models (A, B, C), that best represent the experiment, are presented in Figures 4 and 5. Dimers A and B belong to the H-type organisation, while dimer C is J-type. Simulated ECD spectra of A vs. B and A vs. C have approximately opposite signs, due to different molecular handedness. From lower to higher wavelengths, dimer A ($\alpha = 150°$, $d = 5$ Å) shows a (+/−) ECD profile and negative exciton chirality. In turn, dimers B and C give a (−/+) ECD pattern and positive exciton chirality. The sum of A and B produces the (−/+/−) order of bands located at 610, 647 and 687 nm, respectively. To obtain the (−/+/−) ECD pattern for the A+C combination, it was necessary to multiply the C dimer spectra by an arbitrary factor of 7. Although we do not know the exact H/J ratio in the experiment, the red-shifted absorption maximum indicates the prevalence of J-aggregates, which might justify the selected factor. The final A+B and A+C spectra give a reasonable agreement with the measured data. Only the A+C model (the H+J arrangement type) generated the observed shift of the main absorption band compared to that of the CAX monomer.

Thus, considering the sign, order, and relative intensities of the calculated ECD and UV-vis bands, the simulations are consistent with the CAX-HP and CAX-HA aggregates containing both H and J elements. Furthermore, various computational tests confirmed the dominance of the exciton coupling in the ECD spectra over the structural distortion of a CAX molecule in the dimers (Figure S5). The experimental ECD spectra can be indeed imagined as two or three separate exciton-split Cotton effects (the negative: (+/−) and the positive: (−/+), Figures S10 and S11). CAX molecules in GAG solutions likely form complex arrangements with more parameters determining the chirality in the same way as, for example, protein fibrils. Their filaments may twist to the right, while larger strands of more left-handed components might twist to the left. The dimer models chosen to imitate the structural and spectroscopic properties of CAX aggregates provide spectral features typical of H-type (A and B dimers) and J-type (C dimer) formations, i.e., the blue and red shifts of the main absorption band. Consequently, the CAX-HP and CAX-HA aggregates may contain two or more carotenoid arrange-

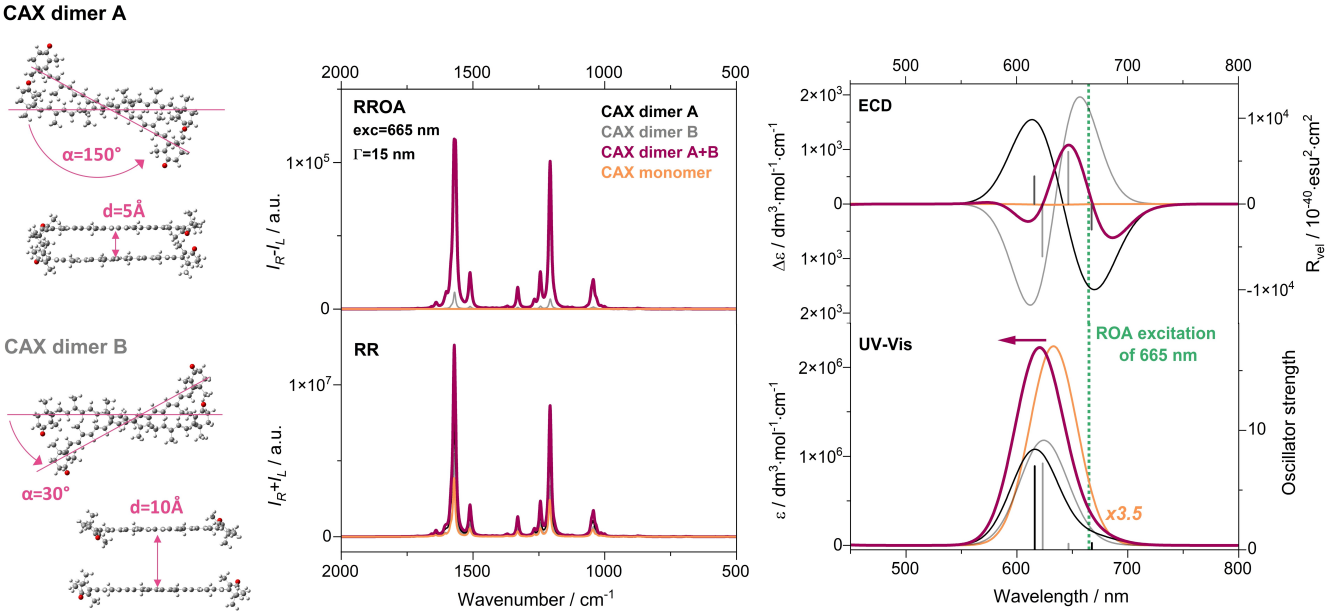

Figure 4. RROA ($I_R - I_L$), RR ($I_R + I_L$), ECD (Δε) and UV-vis (ε) spectra calculated for two types of CAX dimers: A (black line, $\alpha = 150°$, $d_1 = 5$ Å) and B (grey line, $\alpha = 30°$, $d_1 = 10$ Å), where α denotes the torsion angle and d_1 is the distance between the polyene chains. RROA and RR were calculated using the Γ bandwidth of 15 nm. The burgundy line represents theoretical spectra obtained as a sum of A and B. Orange is used for the monomer of the lowest energy CAX conformer. The oscillator and rotatory strengths (R) of electronic transitions are indicated by the black (dimer A) and grey (dimer B) lines. The calculated RROA/RR intensities were scaled by one factor, to approximately correspond to the experimental arbitrary units.

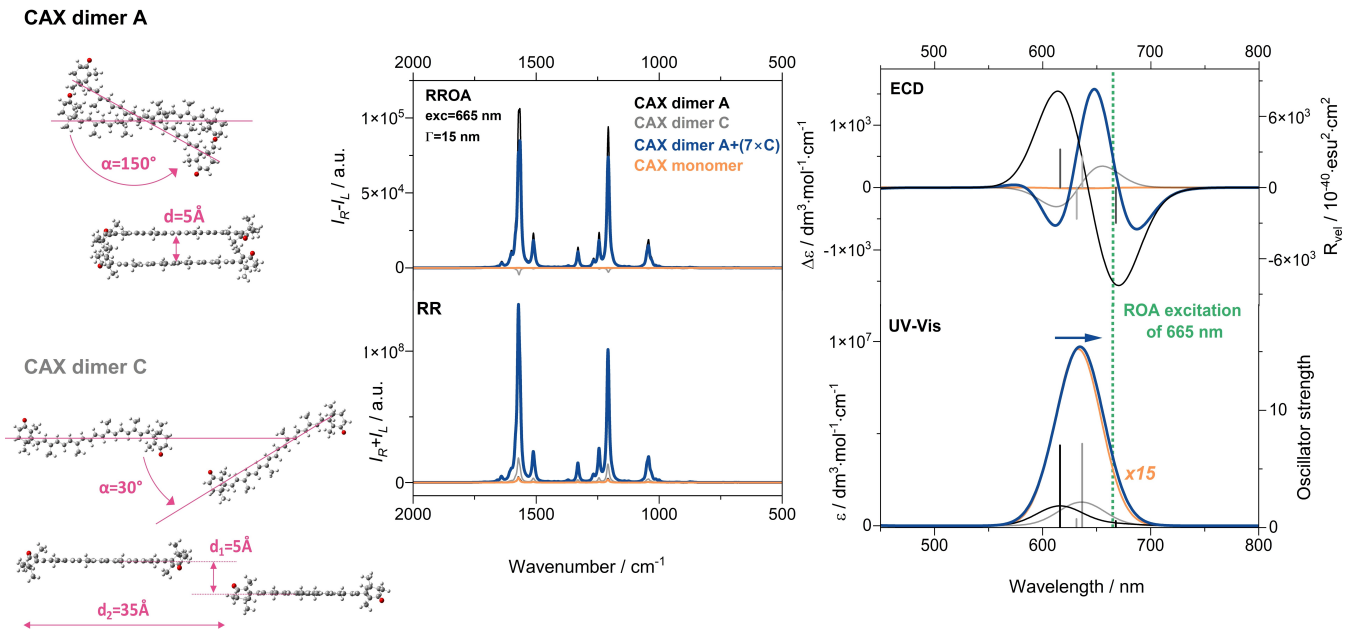

Figure 5. RROA ($I_R - I_L$), RR ($I_R + I_L$), ECD (Δε) and UV-vis (ε) spectra calculated for two types of CAX dimers: A (black line, $\alpha = 150°$, $d_1 = 5$ Å) and C (grey line, $\alpha = 30°$, $d_1 = 5$ Å, $d_2 = 35$ Å), where α denotes the torsion angle d_1 indicates the distance between polyene chains, and d_2 shows the longitudinal shift between two CAX molecules. RROA and RR were calculated using the Γ bandwidth of 15 nm. The blue line represents the theoretical spectra obtained as the sum of A and (7·C). Orange is used for the monomer of the lowest energy CAX conformer. The oscillator and rotatory strength (R) of electronic transitions are marked as black (dimer A) and grey (dimer C) lines.

ments close to the J- and the H-types, perhaps as outer and inner layers of molecules.

The RROA and RR spectra were calculated from the transition electric and magnetic dipole moments of the involved electronic transitions, using a complex bandwidth (damping factor $i\Gamma$, Γ ~5–25 nm). Because of the systematic error of the DFT computations, several excitation lines within 600–700 nm were investigated (SI). The 665 nm excitation coincides with the range of the positive ECD band in the A + B and A + C spectra (Figures 4, 5), the same as the 532 nm line does in the experiment (Figure 2). For this case, all RROA bands for the A and B models are positive, consistent with the experimental data (Figure 3).

As mentioned above, the SES theory cannot be applied here. Still it would be valid for a single CAX dimer under strong resonance conditions (excitation line matching the electronic transition). The positive RROA in the A model originates from a negative ECD transition, and the negative RROA in the C model originates from a positive ECD transition (Figures 4, 5). However, using the 665 nm excitation line and $\Gamma > 10$ nm for the B model, we found that the negative ECD transition affects the RROA sign (positive) more than the closer-lying positive ECD band (Figure S6). This is due to a much higher oscillator (dipole) strength of that transition (UV-vis intensity), as both dipole and rotational strengths play a role in RROA.[42] For the mixed system, the positive RROA prevails even though the overall ECD band profile is positive (Figures 4, 5). Notably, the intensities and signs of the calculated RROA bands are somewhat affected by the bandwidth (damping factor) used in the tensor calculations (Figures S6, S7). Nevertheless, the RROA simulations confirmed qualitatively that the CAX aggregates might indeed have multiple sub-formations of a different chirality.

Finally, the simulations helped to estimate the contribution of the ECD-Raman effect to the measured RROA spectra. For the CAX dimers, the effect appeared as a negative signal but was negligible compared to the positive experimental signal. This justifies the neglection of ECD-Raman in the experimental data (Figures S8, S9).

In conclusion, chirality induction in non-chiral carotenoid (CAX) by chiral polysaccharides (HP and HA) monitored by ECD and ROA spectroscopies has been observed for the first time. The resonance ROA spectra were not affected by the ECD-Raman interference, which DFT calculations confirmed. The ECD and RROA band signs and intensities could also be reproduced by theoretical modelling, albeit with limited accuracy, because of the size and complexity of the systems. The supramolecular chirality induction based on non-covalent interaction among completely achiral CAX molecules is worth attention because it is caused by the natural, chiral environment (GAGs) relevant to living matter, and it could be related to two well-known types of carotenoid arrangements (H and J) described previously.

Supporting Information

The Supporting Information contains complete experimental and computational details and characterisation of the RR and RROA bands for monomeric and aggregated forms of

CAX. Values of CID and g-factor are also provided (Table S2). The authors have cited additional references within the Supporting Information.[51–62]

Acknowledgements

We gratefully acknowledge the National Science Centre in Poland for supporting the experimental part of the study, including preparing supramolecular aggregates, performing and analysing chiroptical measurements under grant nos. 2021/40/C/ST4/00190 and 2019/32/T/ST4/00230 (to MH). We also acknowledge the Grant Agency of the Czech Republic (grant no. 22-04669S; to PB) and the Polish High-Performance Computing infrastructure PLGrid (HPC Centers: ACK Cyfronet AGH) for providing computer facilities and support under computational grant no. PLG/2023/016719 (to GZ). MD calculations were performed with the computational resources provided by e-INFRA CZ project no. 90254, supported by the Ministry of Education, Youth and Sports of the Czech Republic (to VA).

Conflict of Interest

The authors declare no conflict of interest.

Data Availability Statement

The data that support the findings of this study are available from the corresponding author upon reasonable request.

Keywords: resonance Raman optical activity · circular dichroism · density functional theory · chirality induction · canthaxanthin · heparin · hyaluronic acid

[1] T. Maoka, *J. Nat. Med.* **2020**, *74*, 1–16.
[2] S. Köhn, H. Kolbe, M. Korger, C. Köpsel, B. Mayer, H. Auweter, E. Lüddecke, H. Bettermann, H.-D. Martin, in *Carotenoids*, Vol. 4 (Eds.: G. Britton, S. Liaaen-Jensen, H. Pfander), Birkhäuser Basel, Basel **2008**, pp. 53–98.
[3] J. Hempel, C. N. Schädle, S. Leptihn, R. Carle, R. M. Schweiggert, *J. Photochem. Photobiol. A* **2016**, *317*, 161–174.
[4] G. Zajac, E. Machalska, A. Kaczor, J. Kessler, P. Bouř, M. Baranska, *Phys. Chem. Chem. Phys.* **2018**, *20*, 18038–18046.
[5] M. Liu, L. Zhang, T. Wang, *Chem. Rev.* **2015**, *115*, 7304–7397.
[6] L. Wang, N. Suzuki, J. Liu, T. Matsuda, N. A. A. Rahim, W. Zhang, M. Fujiki, Z. Zhang, N. Zhou, X. Zhu, *Polym. Chem.* **2014**, *5*, 5920–5927.
[7] P. Rizzo, S. Abbate, G. Longhi, G. Guerra, *Opt. Mater.* **2017**, *73*, 595–601.
[8] K. Watanabe, H. Iida, K. Akagi, *Adv. Mater.* **2012**, *24*, 6451–6456.
[9] G. Zajac, A. Kaczor, A. Pallares Zazo, J. Mlynarski, M. Dudek, M. Baranska, *J. Phys. Chem. B* **2016**, *120*, 4028–4033.
[10] M. Dudek, G. Zajac, A. Kaczor, M. Baranska, *J. Phys. Chem. B* **2016**, *120*, 7807–7814.
[11] G. Zajac, J. Lasota, M. Dudek, A. Kaczor, M. Baranska, *Spectrochim. Acta Part A* **2017**, *173*, 356–360.
[12] M. Dudek, G. Zajac, A. Kaczor, M. Baranska, *J. Raman Spectrosc.* **2017**, *48*, 673–679.
[13] M. Dudek, E. Machalska, T. Oleszkiewicz, E. Grzebelus, R. Baranski, P. Szcześniak, J. Mlynarski, G. Zajac, A. Kaczor, M. Baranska, *Angew. Chem. Int. Ed.* **2019**, *58*, 8383–8388.
[14] S. Huang, H. Yu, Q. Li, *Adv. Sci.* **2021**, *8*, 2002132.
[15] M. Fujiki, *Symmetry (Basel).* **2014**, *6*, 677–703.
[16] S. Jiang, Y. Zhao, L. Wang, L. Yin, Z. Zhang, J. Zhu, W. Zhang, X. Zhu, *Polym. Chem.* **2015**, *6*, 4230–4239.
[17] T. Miao, X. Cheng, Y. Guo, G. Zhang, W. Zhang, *Giant* **2023**, *14*, 100161.
[18] T. Yamaguchi, T. Kimura, H. Matsuda, T. Aida, *Angew. Chem. Int. Ed.* **2004**, *43*, 6350–6355.
[19] M. Wolffs, S. J. George, Ž. Tomović, S. C. J. Meskers, A. P. H. J. Schenning, E. W. Meijer, *Angew. Chem. Int. Ed.* **2007**, *46*, 8203–8205.
[20] W. L. Noorduin, A. A. C. Bode, M. van der Meijden, H. Meekes, A. F. van Etteger, W. J. P. van Enckevort, P. C. M. Christianen, B. Kaptein, R. M. Kellogg, T. Rasing, E. Vlieg, *Nat. Chem.* **2009**, *1*, 729–732.
[21] J. Kim, J. Lee, W. Y. Kim, H. Kim, S. Lee, H. C. Lee, Y. S. Lee, M. Seo, S. Y. Kim, *Nat. Commun.* **2015**, *6*, 6959.
[22] N. Micali, H. Engelkamp, P. G. van Rhee, P. C. M. Christianen, L. M. Scolaro, J. C. Maan, *Nat. Chem.* **2012**, *4*, 201–207.
[23] B. A. Rebelo, S. Farrona, M. R. Ventura, R. Abranches, *Plants* **2020**, *9*, 1039.
[24] A. Sujak, *Cell. Mol. Biol. Lett.* **2009**, *14*, 395–410.
[25] H. Sodhi, A. Panitch, *Biomol. Eng.* **2021**, *11*, 29.
[26] T. Sagawa, H. Tobata, H. Ihara, *Chem. Commun.* **2004**, 2090–2091.
[27] F. E. Stanley, A. M. Warner, S. M. Gutierrez, A. M. Stalcup, *Biochem. Biophys. Res. Commun.* **2009**, *388*, 28–30.
[28] D. Fedunova, P. Huba, J. Bagelova, M. Antalik, *Gen. Physiol. Biophys.* **2013**, *32*, 215–219.
[29] S. Vilasi, R. Sarcina, R. Maritato, A. De Simone, G. Irace, I. Sirangelo, *PLoS One* **2011**, *6*, e22076.
[30] M. Sebastiao, N. Quittot, I. Marcotte, S. Bourgault, *Biochemistry* **2019**, *58*, 1214–1225.
[31] F. Zsila, S. A. Samsonov, M. Maszota-Zieleniak, *J. Phys. Chem. B* **2020**, *124*, 11625–11633.
[32] L. Satish, S. Santra, M. V. Tsurkan, C. Werner, M. Jana, H. Sahoo, *Int. J. Biol. Macromol.* **2021**, *182*, 2144–2150.
[33] B. J. Foss, H. R. Sliwka, V. Partali, C. Köpsel, B. Mayer, H. D. Martin, F. Zsila, Z. Bikadi, M. Simonyi, *Chem. A Eur. J.* **2005**, *11*, 4103–4108.
[34] H. Sato, *Phys. Chem. Chem. Phys.* **2020**, *22*, 7671–7679.
[35] T. Wu, G. Li, J. Kapitán, J. Kessler, Y. Xu, P. Bouř, *Angew. Chem.* **2020**, *132*, 22079–22082.
[36] E. Machalska, G. Zajac, A. J. Wierzba, J. Kapitán, T. Andruniów, M. Spiegel, D. Gryko, P. Bouř, M. Baranska, *Angew. Chem. Int. Ed.* **2021**, *60*, 21205–21210.
[37] T. Wu, J. Kapitán, P. Bouř, *J. Phys. Chem. Lett.* **2022**, *13*, 3873–3877.
[38] F. C. Spano, *J. Am. Chem. Soc.* **2009**, *131*, 4267–4278.
[39] J. Olšina, M. Durchan, B. Minofar, T. Polívka, T. Mančal, *arXiv-1208 4958v1 [physics.chem-ph]* **2012**, 1–11.
[40] M. Fuciman, M. Durchan, V. Šlouf, G. Keşan, T. Polívka, *Chem. Phys. Lett.* **2013**, *568–569*, 21–25.
[41] M. Simonyi, Z. Bikádi, F. Zsila, J. Deli, *Chirality* **2003**, *15*, 680–698.
[42] M. Kasha, H. R. Rawls, M. Ashraf El-Bayoumi, *Pure Appl. Chem.* **1965**, *11*, 371–392.
[43] N. Berova, L. Di Bari, G. Pescitelli, *Chem. Soc. Rev.* **2007**, *36*, 914–931.
[44] G. Pescitelli, L. Di Bari, N. Berova, *Chem. Soc. Rev.* **2014**, *43*, 5211–5233.

[45] N. Hachlica, M. Stefańska, M. Mach, M. Kowalska, P. Wydro, A. Domagała, J. Kessler, G. Zając, A. Kaczor, *Small* **2024**, 2306707.
[46] L. A. Nafie, *Chem. Phys.* **1996**, *205*, 309–322.
[47] L. A. Nafie, *Chirality* **2020**, *32*, 667–692.
[48] G. Zając, P. Bouř, *J. Phys. Chem. B* **2022**, *126*, 355–367.
[49] A. Baiardi, J. Bloino, V. Barone, *J. Chem. Theory Comput.* **2018**, *14*, 6370–6390.
[50] N. Tschirner, M. Schenderlein, K. Brose, E. Schlodder, M. A. Mroginski, C. Thomsen, P. Hildebrandt, *Phys. Chem. Chem. Phys.* **2009**, *11*, 11471–11478.
[51] D. A. Case, I. Y. Ben-Shalom, S. R. Brozell, D. S. Cerutti, I. I. I. T. E. Cheatham, V. W. D. Cruzeiro, T. A. Darden, R. E. Duke, D. Ghoreishi, M. K. Gilson, H. Gohlke, A. W. Goetz, D. Greene, R. Harris, N. Homeyer, Y. H. Ang, S. Izadi, A. Kovalenko, T. Kurtzman, T. S. L. S. LeGrand, P. Li, C. Lin, J. Liu, T. Luchko, R. Luo, D. J. Mermelstein, K. M. Merz, Y. Miao, G. Monard, C. Nguyen, H. Nguyen, I. Omelyan, A. Onufriev, F. Pan, R. Qi, D. R. Roe, A. Roitberg, C. Sagui, S. Schott-Verdugo, J. Shen, C. L. Simmerling, J. Smith, R. Salomon-Ferrer, J. Swails, R. C. Walker, J. Wang, H. Wei, R. M. Wolf, X. Wu, L. Xiao, D. M. York, P. A. Kollman, *AMBER 2018*, University Of California, San Francisco **2018**.
[52] B. Mulloy, M. J. Forster, C. Jones, D. B. Davies, *Biochem. J.* **1993**, *293*, 849–858.
[53] P. Bouř, T. A. Keiderling, *J. Chem. Phys.* **2002**, *117*, 4126–4132.
[54] L. D. Barron, *Molecular Light Scattering and Optical Activity*, Cambridge University Press **2009**.
[55] P. Bouř, P. Maloň, *MCM Molecular Graphics*, Academy Of Sciences, Prague **2011**.
[56] C. I. Bayly, P. Cieplak, W. Cornell, P. A. Kollman, *J. Phys. Chem.* **1993**, *97*, 10269–10280.
[57] F.-Y. Dupradeau, A. Pigache, T. Zaffran, C. Savineau, R. Lelong, N. Grivel, D. Lelong, W. Rosanski, P. Cieplak, *Phys. Chem. Chem. Phys.* **2010**, *12*, 7821–7839.
[58] E. Vanquelef, S. Simon, G. Marquant, E. Garcia, G. Klimerak, J. C. Delepine, P. Cieplak, F. Y. Dupradeau, *Nucleic Acids Res.* **2011**, *39*, W511–W517.
[59] F. Wang, J.-P. Becker, P. Cieplak, F.-Y. Dupradeau, *R. E. D. Python: Object Oriented Programming for Amber Force Fields*, Université De Picardie—Jules Verne, Sanford Burnham Prebys Medical Discovery Institute **2013**.
[60] M. J. Frisch, G. W. Trucks, H. B. Schlegel, G. E. Scuseria, M. A. Robb, J. R. Cheeseman, G. Scalmani, V. Barone, G. A. Petersson, H. Nakatsuji, X. Li, M. Caricato, A. V. Marenich, J. Bloino, B. G. Janesko, R. Gomperts, B. Mennucci, H. P. Hratchian, J. V. Ortiz, A. F. Izmaylov, J. L. Sonnenberg, D. Williams-Young, F. Ding, F. Lipparini, F. Egidi, J. Goings, B. Peng, A. Petrone, T. Henderson, D. Ranasinghe, V. G. Zakrzewski, J. Gao, N. Rega, G. Zheng, W. Liang, M. Hada, M. Ehara, K. Toyota, R. Fukuda, J. Hasegawa, M. Ishida, T. Nakajima, Y. Honda, O. Kitao, H. Nakai, T. Vreven, K. Throssell, J. A. Montgomery Jr., J. E. Peralta, F. Ogliaro, M. J. Bearpark, J. J. Heyd, E. N. Brothers, K. N. Kudin, V. N. Staroverov, T. A. Keith, R. Kobayashi, J. Normand, K. Raghavachari, A. P. Rendell, J. C. Burant, S. S. Iyengar, J. Tomasi, M. Cossi, J. M. Millam, M. Klene, C. Adamo, R. Cammi, J. W. Ochterski, R. L. Martin, K. Morokuma, O. Farkas, J. B. Foresman, D. J. Fox, *Gaussian 16, Revision C.01*, Gaussian, Inc, Wallingford CT **2016**.
[61] G. Zajac, A. Kaczor, S. Buda, J. Młynarski, J. Frelek, J. C. Dobrowolski, M. Baranska, *J. Phys. Chem. B* **2015**, *119*, 12193–12201.
[62] L. Martínez, R. Andrade, E. G. Birgin, J. M. Martínez, *J. Comput. Chem.* **2009**, *30*, 2157–2164.

Manuscript received: February 2, 2024
Accepted manuscript online: March 22, 2024
Version of record online: ■■, ■■

Communications

Noncovalent Interactions

M. Halat,* G. Zając, V. Andrushchenko, P. Bouř,* R. Baranski, K. Pajor, M. Baranska* e202402449

Induced Chirality in Canthaxanthin Aggregates Reveals Multiple Levels of Supramolecular Organization

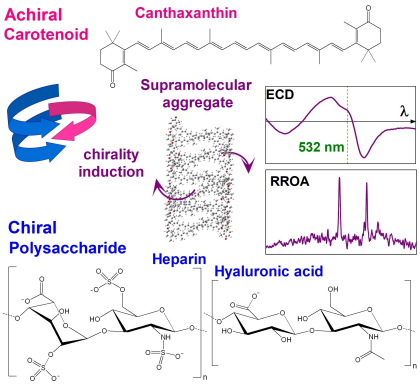

Mixing chiral polysaccharides with the achiral carotenoid canthaxanthin (CAX) leads to a unique chirality induction, with strong optical activity visible in the electronic circular dichroism (ECD) and resonance Raman optical activity (RROA) spectra. Interpretation of the data using density functional theory (DFT) and molecular dynamics (MD) modelling suggests an intricate supramolecular structure with multiple carotenoid–carotenoid interactions.